Journal of Materials Chemistry B

ROYAL SOCIETY OF CHEMISTRY

PAPER

View Article Online
View Journal | View Issue

Cite this: J. Mater. Chem. B, 2025, 13, 8105

Quaternary ammonium-functionalized carbon nanotubes/alginate nanocomposite hydrogels support myoblast growth and differentiation†

Ludovica Ceroni,‡[a] Tianqi Feng,‡[b] Laura Calvillo,[a] Stefano Casalini,[a] Patrick Van Rijn*[b] and Enzo Menna*[a]

Carbon nanotube (CNT) composite hydrogels are promising materials for tissue engineering due to the biocompatibility of the matrix and the electrical conductivity of the filler, which is crucial for promoting the growth and functions in electroactive tissues. While pristine CNTs are insoluble, we synthesized and fully characterized a water-soluble CNT derivative (fCNT) bearing quaternary ammonium groups, and we homogeneously dispersed it within alginate-based hydrogels. Through external and internal gelation we obtained two plain and two fCNT-filled hydrogels (HG1 and HG2 and HG1-fCNT and HG2-fCNT, respectively), and we compared the physical properties of the four different materials. A measurement setup and an approach were specifically designed for the electrical characterization of our hydrogel samples, showing that the addition of a low amount (0.1 mg mL^{-1}) of fCNT enhanced the conductivity of the hydrogel from internal gelation (HG2-fCNT) by more than one order of magnitude, from 5.7×10^{-10} to 2.8×10^{-8} S cm^{-1}. Even more interestingly, HG2-fCNT featured a faster transmission of low frequency signals (with time scales from 1 ms to 100 ms, typical of electroactive biological tissues) than the other samples. Finally, the behavior of the four hydrogels as scaffolds for muscle tissue engineering was compared through studies of myoblast viability, proliferation, and differentiation. A relevant improvement in differentiation (more than doubling the number and area of myotubes and the fusion index) was obtained by adding the fCNT in the case of HG2-fCNT, in line of its superior electrical properties. These outcomes hint at the feasibility of using the fCNT combined with the alginate hydrogel in order to support the myoblast growth and proliferation.

Received 17th March 2025,
Accepted 23rd May 2025

DOI: 10.1039/d5tb00601e

rsc.li/materials-b

1. Introduction

In the field of tissue engineering, there is particular interest in creating a stimulating environment for cell growth and differentiation of specific tissues and organs with the intention of repairing or replacing them.[1] Scaffolds for tissue engineering are biomaterials designed to exhibit customizable properties with the purpose of sustaining cell functions and enhancing cell responses.[2] These materials should exhibit a controllable microstructure and adequate porosity, thus allowing for the transport of nutrients, cell migration within the construct, and the diffusion of waste or the exit of degradation products.[3] Moreover, the mechanical properties of the scaffolds are of crucial importance in ensuring adequate support for the growing tissue. Ideally, the stiffness of the scaffold should be consistent with the anatomical site being treated.[2] Certain tissues could additionally benefit from the specific electric properties of the environment. Indeed, electroactive tissues rely on signal transduction based on electrochemical potential for their development and functions. For instance, ventricular muscle, nerve, lung, cardiac, and skeletal muscle display electrical conductivity ranging between 0.03 and 0.6 S m^{-1},[4] and their cellular functions, including growth, migration, adhesion, proliferation and differentiation, can be modulated by electrical signals. In this case, biomaterials with electroactive components represent a new generation of "smart" biomaterials, which enable the direct transfer of electrical and electromechanical stimuli to cells with or without external electrical stimulation.[5] For this reason, carbon-based materials are promising candidates as building blocks in scaffolds for tissue engineering. Specifically, carbon nanotubes (CNTs) have attracted much attention thanks to their unique combination

[a] Department of Chemical Sciences, University of Padova & INSTM, Via Marzolo 1, 35131, Padova, Italy. E-mail: enzo.menna@unipd.it
[b] Department of Biomaterials & Biomedical Technology, University Medical Center Groningen, University of Groningen, Groningen, The Netherlands. E-mail: p.van.rijn@umcg.nl

† Electronic supplementary information (ESI) available. See DOI: https://doi.org/10.1039/d5tb00601e

‡ These authors contributed equally to this work as first authors.

of chemical and physical properties.[6] Due to their extended C-sp^2 structure, they exhibit high electrical conductivity and modulation of electrostatic potential that can be exploited in the formation of electroactive composite materials, which have already been extensively studied especially for the regeneration of cardiac and neuronal tissues.[7–11] CNTs did not demonstrate only support of cell growth but also enhancement of cell adhesion to the substrate, proliferation, and differentiation, in particular osteogenic, neuronal and myogenic.[12–15] Furthermore, CNTs demonstrated to function as a reinforcing agent within polymer matrices, thereby modulating the stiffness of the composite material to meet specific requirements and introducing micro- and nano-scale morphologies.[16]

In the specific area of muscle tissue engineering, myogenic cells are isolated from the tissue and made to proliferate and fuse into myotubes in 2D cultures that can then rearrange in parallel and organize in 3D to obtain new engineered muscle tissue.[17] The most frequently employed scaffolds for this purpose are hydrogels, thanks to their structural and compositional resemblance to the natural extracellular matrix (ECM), as well as their capacity to facilitate cell proliferation and survival.[18] These materials possess a soft and flexible texture, similar to that of living tissues, and a high level of hydrophilicity due to the presence of hydrophilic groups (*e.g.* –NH_2, –COOH, –OH, and –$CONH_2$) which ensure the bidirectional flow of water or biological fluids.[19] Alginate, in particular, is a well-known hydrogel based on polysaccharides from natural sources that differ in the relative amount of β-D-mannuronic acid (M) and α-L-guluronic acid (G) residues and is typically crosslinked by Ca^{2+} ions between the G units.[20] This material is biocompatible, biodegradable, biologically inert, and it is characterized by a high-water content.[18,21] Alginate exhibits an adjustable shape and porosity, fast gelling behaviour and the ability to adapt the mechanical properties to mimic those of natural tissues depending on the type, amount and crosslinking density of the polymer in the hydrogel.[22–24] Thanks to these properties, it was already used for organ repair, for example in bone[24,25] and cartilage tissue engineering.[26,27]

As skeletal muscle tissues possess electrical excitable properties, the incorporation of CNTs as fillers within hydrogel matrices results in the formation of electroactive composite materials which facilitate the local transmission of electrical stimuli, thereby enhancing cell responses and tissue regeneration. CNT-based materials have been successfully shown to contribute to myogenesis and muscle tissue recovery due to their electrical and mechanical properties.[15,28] The problem associated with the use of carbon nanostructures is that they are highly hydrophobic and tend to aggregate in any solvent, and in particular in water, through π–π stacking and van der Waals interactions.[29] Chemical modification of CNTs is an effective strategy to limit aggregation and promote homogeneous dispersion of the nanostructure in matrices and to obtain hybrid scaffolds with uniform properties.[30] Moreover, several studies suggest that the functionalization of CNTs could enhance their biocompatibility and biodegradability, thus making them safer for a biomedical use.[31] Indeed, through covalent functionalization, we previously obtained CNT derivatives soluble in organic solvents and we used them as fillers in polymer-based scaffolds for the proliferation of the human neuronal precursor cell line SH-SY5Y and neurite extension.[9,32] We also reported on the synthesis of water-soluble CNT derivatives that could be effectively dispersed in oxidized polyvinylalcohol matrices. The resulting composites showed promising features as conductive nerve conduits.[10] Functionalisation can also be considered a strategy for modulating the interactions of the nanostructure with the matrix. For example, when charges are introduced onto the surface of CNTs, electrostatic interactions can be initiated with charged polymers, thus enabling the grafting of CNTs into the matrix and preventing their uncontrolled release towards the cell environment. A similar strategy, based on charge interactions between a positively charged polyelectrolyte and alginate, was successfully employed in the past.[33]

In the present study, we focus on the functionalization of multi-walled CNTs with positively charged quaternary ammonium groups to obtain a water-dispersible CNT derivative (fCNT), which specifically promotes potential interactions with carboxylate units of the alginate chains. The hybrid scaffolds were prepared with the aim of improving electrical response, weight retention and mechanical stability. Moreover, two distinct alginate gelation methods were employed and subsequently compared on the basis of their divergent physical properties. Finally, the response of myoblasts to these scaffolds was studied, with the ultimate purpose of obtaining well-suited materials that resemble the structure and mechanical properties of muscle tissues.

2. Experimental

Multi-walled CNTs (outer diameter: 8–15 nm and length: 0.5–2 μm), purity >95%, were purchased from ACS Material (Pasadena, CA, USA). Sodium alginate with a low viscosity between 5.0 and 40.0 cps (Product Number: W201502) and solvents and reagents used in the synthesis procedures were all purchased from Sigma-Aldrich (Milan, Italy). Concerning the cell experiments, DMEM-HG, fetal bovine serum, pen/streptomycin, insulin–transferrin–selenium were purchased from Gibco, and dexamethasone, paraformaldehyde and live/dead staining were purchased from Sigma-Aldrich.

2.1. Synthesis of CNT-PhN$(CH_3)_3^+$ (fCNT)

Multi-walled CNTs (70.0 mg, 5.82 mmol of carbon) were mixed with a solution of 4-amino-*N*,*N*,*N*-trimethylbenzene ammonium iodide (810.51 mg, 2.91 mmol) in 17 mL of Milli-Q water. The reaction mixture was heated to 80 °C under nitrogen flux and magnetic stirring; then, isopentyl nitrite (0.824 mL, 5.82 mmol) was added. After 4 hours, the reaction mixture was allowed to cool to room temperature. The dispersion was filtered on a Millipore PC 0.1 μm membrane (VCTP), and the product was washed on the filter with 50 mL of distilled water and then removed from the filter through sonication in 50 mL of distilled

water. The filtration/washing procedure was repeated four times using water : methanol (1 : 1) and one time using methanol. The methanol dispersion was finally dried under nitrogen flux to afford the multi-walled CNT derivative (fCNT) as a solid black powder.

2.2. Characterization of fCNT

2.2.1. Raman spectroscopy. Raman measurements were performed on pristine CNTs and fCNT with an Invia Renishaw Raman microspectrometer (50× objective). The samples were placed on glass micro slides (Corning), fixed with tape and irradiated for 10 seconds using the 633 nm line of a He–Ne laser with a low laser power at room temperature. The reported values were the average of 3 measurements taken on different portions of the sample.

2.2.2. X-ray photoelectron spectroscopy (XPS). The XPS spectra of pristine CNTs and fCNT were recorded using a custom-made UHV system working at a base pressure of 10^{-10} mbar, equipped with an Omicron EA125 electron analyzer and an Omicron DAR 400 X-ray source with a dual Al–Mg anode. Core-level photoemission spectra (C 1s and N 1s regions) were collected with a non-monochromatized Al Kα X-ray source (1486.3 eV) in normal emission at room temperature. Measurement parameters were set at 0.1 eV steps, 0.5 s collection time, and 20 eV pass energy.

2.2.3. Thermogravimetric analysis (TGA). TGA of pristine CNTs and fCNT was performed using a TGA Q5000IR instrument (TA instruments, New Castle, DE, USA) on a 100 μL platinum HT TAG pan in a nitrogen atmosphere. The measures were carried out at 10 °C min^{-1} up to 1000 °C subsequently to an isotherm at 100 °C for 10 min to remove the possible traces of residual solvents. The thermograms were processed using Universal Analysis software.

2.2.4. Preparation of fCNT standard dispersion. fCNT derivative (5 mg) was dispersed in Milli-Q water (2.5 mL) by pulsed microtip sonication for 1 minute (Misonix S3000 Sonicator; time on = 3 s, time off = 3 s, power level = 2 (4–6 W)) and then centrifuged (Thermo Electron Corporation, Waltham, MA, USA) at 5000 rpm for 10 min to precipitate the less dispersable fraction. The supernatant was filtered over cotton wool to remove fluffy, large and lightweight aggregates potentially non-precipitated during the centrifugation process and results in a filtrate which is the fCNT standard dispersion.

2.2.5. Measurement of dispersibility. The dispersibility in water of fCNT derivative is defined as the concentration (m/V) of the standard dispersion obtained through the above-described procedure. The concentration was measured through the following procedure. A known volume (1 mL) of dispersion was drop cast on a calibrated pan and a TGA measurement consisting of an isotherm at 100 °C for 15 minutes in air provided the dry weight used to calculate the m/V concentration.

2.2.6. Dynamic light scattering (DLS) and zeta potential (ZP). The fCNT standard dispersion (100 μL) was added to Milli-Q water (1.0 mL) in disposable plastic cuvettes with an optical path of 1 cm for DLS analysis. The DLS measurement was performed using a Zetasizer Nano S analyzer (Malvern Instruments, Malvern, UK) setting the measurement angle at 173°, backscatter (NIBS default), water as the solvent, temperature at 25 °C and equilibration time at 120 s. The reported value was an average of 3 measurements of 11 runs each, with a run duration of 10 s.

The fCNT standard dispersion (100 μL) and a solution of 1 mg mL^{-1} of NaCl in water (160 μL) were added to Milli-Q water (700 μL) and placed in a folded capillary cell for zeta potential analysis. The ZP measurement was carried out in NaCl 30 mM, equilibrating at 25 °C for 120 s. The Smoluchowski equation was used as a theoretical model for the measurement and the resulting value was an average of 3 measurements of 10–100 runs each.

2.2.7. DLS and ZP of alginate@fCNT. The mixture of alginate and fCNT for the DLS measurements (alginate@fCNT) was prepared starting from a stock dispersion of 2 mg mL^{-1} of fCNT (obtained just through pulsed microtip sonication for 3 min) and a stock solution of 4 w/v% of sodium alginate in Milli-Q water. 0.5 mL of fCNT stock dispersion was mixed with 0.19 mL of alginate stock solution and 0.31 mL of Milli-Q water to obtain 1 mL of alginate@fCNT dispersion (containing 1 mg fCNT and 7.5 mg alginate). In order to remove the excess of alginate, thus leaving only the fraction of the polymer wrapped on fCNT particles, the following procedure was employed. The alginate@fCNT dispersion was further diluted with 4 mL of Milli-Q water, kept in an ultrasonic bath for 10 minutes and subsequently centrifuged at 20 000 RCF for 10 minutes. The supernatant was removed and the precipitate was further washed by repeating the same procedure five more times. Then, an alginate@fCNT dispersion in 1 mL of Milli-Q water was bath sonicated for 10 minutes and diluted 10 times for the measurements. For comparison, a control sample was also prepared according to the same procedure starting from the fCNT stock dispersion (without alginate). The DLS size and ZP analysis were carried out using a Zetasizer Nano-ZS (Malvern Instruments, Worcestershire, UK) using a clear disposable zeta cell, setting the scattering angle at 173°, equilibrating at 25 °C for 120 s. The reported value of the hydrodynamic mean diameter was an average of 3 measurements of 11 runs each, with a run duration of 10 s. For data evaluation, the Smoluchowski equation was used as a theoretical model.

2.3. Preparation of the scaffolds HG1, HG1-fCNT, HG2, and HG2-fCNT

Four alginate hydrogels, without and with fCNT as a filler, were prepared following two different gelation techniques, namely the external gelation (hereafter HG1 and HG1-fCNT) and the internal gelation (hereafter HG2 and HG2-fCNT). Table 1 summarizes reagents and quantities for both approaches. Samples were prepared in the form of discs using a circular polydimethylsiloxane (PDMS) mold previously fabricated. All solutions were prepared with Milli-Q water. The external gelation was carried out by pouring 1 mL of alginate solution 2 w/v% in the circular PDMS mold; then, a dialysis membrane was positioned on top of the alginate solution followed by a transwell

Table 1 Parameters of alginate scaffold fabrication by external and internal gelation techniques

	External gelation		Internal gelation	
Reagents	HG1	HG1-fCNT	HG2	HG2-fCNT
fCNT (w/v%)	—	0.01 (0.1 mg mL^{-1})	—	0.01 (0.1 mg mL^{-1})
Alginate (w/v%)	2		2	
$CaCO_3$ (mM)	—		60	
GDL (mM)	—		120	
$CaCl_2$ (mM)	50, incubate 23 h 4 °C		—	

insert. Next, 3 mL of a 50 mM $CaCl_2$ solution were poured into the transwell and the system was left to equilibrate in the fridge overnight to allow Ca^{2+} ions to pass through the membrane and crosslink the alginate chains. Instead, for the internal gelation protocol, 0.5 mL of alginate solution 4 w/v%, 0.1 mL of Milli-Q water and 0.2 mL of a 300 mM dispersion of $CaCO_3$ were vortexed and mixed in an ultrasonic bath. Once $CaCO_3$ was homogeneously dispersed in the alginate solution, 0.2 mL of a 600 mM solution of glucono-delta-lactone (GDL) freshly prepared was added. The mixture was finally poured into a circular PDMS mold, left at room temperature for 5 hours to make sure that the hydrogel is formed and then stored in the fridge until use.

For the preparation of hybrid hydrogels, a fCNT stock dispersion of 1 mg mL^{-1} was prepared through tip sonication for 3 minutes. Then, before gelation, the stock dispersion was added to the alginate solution to achieve the final fCNT concentration of 0.1 mg mL^{-1}.

2.4. Characterization of the scaffolds

2.4.1. Scanning electron microscopy (SEM). SEM analysis was performed on freeze-dried samples. The cross-section was cut with a scalpel, placed on a metallic stub using carbon tape and sputtered with a thin gold layer (Scancoat six, 10 nm). SEM images were acquired with a Zeiss Sigma HD microscope, equipped with a Schottky FEG source, a backscattered electron detector and two secondary electron detectors (InLens and Everhart Thornley). Analysis was performed in a high vacuum at 2×10^{-5} mbar.

2.4.2. Scaffold mechanical properties. The elastic modulus was evaluated using a low-load compression tester (LLCT) which was equipped with a linear positioning stage (Intellistage M-511.5IM, Physik Instrument) mounted vertically which moves the top plate/plunger and a load cell (Wipotec, SW 50/300) kept horizontally on which the material to be measured was placed and controlled using a PC using the LabVIEW™ 2014 program.[34] The elastic modulus of the hydrogels was evaluated through the uniaxial compression test and determined as the slope between the stress and strain curves. The samples were compressed with a 2.5 mm diameter plunger in three different spots at 37 °C, setting the object touch speed at 5.0 μm s^{-1}, the maximum deformation at 10%, the deformation units at 5.0% s^{-1} and waiting 20 seconds after the deformation.

2.4.3. Gel response to the cell culture medium. Alginate scaffolds were prepared as reported in section 2.3. The calcium-enhanced cell culture medium was prepared in DMEM-HG (high glucose) by mixing 2 mL of 500 mM $CaCl_2$ solution, 20% of FBS and 1% of P/S (penicillin/streptomycin). The hydrogel samples were soaked in culture medium and kept in an incubator at 37 °C for 10 days, changing the medium every day. The weight, the size and the elastic modulus of the samples were recorded after 1, 2, 3, 7 and 10 days. The weight percentage was reported with respect to the initial weight of the samples. The elastic modulus was evaluated using a low-load compression tester (LLCT) as reported in the previous Section 2.4.2.

2.4.4. Scaffold electrical properties. HG1, HG2, HG1-fCNT and HG2-fCNT were manually placed on interdigitated electrodes (IDEs) on a glass substrate (G-IDE222 purchased from DropSens, Metrohm) which were connected to a potentiostat (Metrohm Autolab Potentiostat–Galvanostat PGSTAT302N). More specifically, IDEs were composed of 52 pairs of digits, 10 μm wide and equally spaced (*viz.* 10 μm). The total area was 4 mm^2; in contrast, the area in between the interdigitated electrodes was 1.75 mm^2 and the meandering path was 17.47 cm long. The electrochemical cell was composed of these IDEs, which act as working and counter electrodes. Aiming at a comprehensive and systematic comparison between the pristine alginate hydrogel and the one filled with fCNT, three different types of techniques were chosen: (i) cyclic voltammetry (CV), (ii) chronoamperometry (CA) and (iii) electrochemical impedance spectroscopy (EIS). Concerning CV, the potential ranged from −200 mV to 200 mV (*i.e.* the starting and ending potential was −200 mV, whereas 200 mV was the upper part of the potential ramp) by changing systemically the scan rate, namely from 50 mV s^{-1} to 500 mV s^{-1}. Each CV measurement was performed after previously defining the open circuit potential (OCP), since no reference electrode was used. The widely accepted formula to be used for the specific capacitance extraction is the following: $C = \frac{\int I \mathrm{d}V}{2m \cdot \Delta V \cdot v}$ where I is the current, dV is the scanned potential, m is the mass of the hydrogel (*viz.* m_{HG1} = 22.1 mg; $m_{HG1\text{-}fCNT}$ = 22.9 mg; m_{HG2} = 27.1 mg; $m_{HG2\text{-}fCNT}$ = 27.7 mg), ΔV is the potential range (*i.e.* 400 mV), and v is the scan rate (*i.e.* from 50 mV s^{-1} to 500 mV s^{-1}). Regarding CA, we applied a step potential of 200 mV for 5 seconds, and the acquisition time was 10 ms. Finally, EIS was performed by applying a series of sinusoidal waves featuring an amplitude of 10 mV and a set point potential of 0 V (*versus* OCP). We selected a range of frequencies from 10^5 to 10^{-1} Hz.

The whole batch of electrochemical measurements was performed by sealing the sample holder thereby keeping wet the surrounding environment from water vapor. This technical aspect preserved the overall hydration of the hydrogel, and it allowed us to avoid keeping a droplet of solution on top of it.

2.5. Cell experiments

2.5.1. Cell culture. Human myoblasts were kindly provided by Prof. Marco Harmsen (Faculty of Medical Sciences, UMCG, Groningen) and were already used in our previous studies.[35,36]

For the current studies, clone V49 was used between Passages 10 and 13. Cells were cultured in growth medium composed of DMEM-HG, 20% fetal bovine serum, and 1% pen/streptomycin under 5% CO_2 and 37 °C. For the differentiation stage, upon reaching confluency, the medium was changed to differentiation medium which included DMEM-HG, 1% fetal bovine serum, 1% pen/streptomycin, 1% insulin–transferrin–selenium, and 1% dexamethasone. All hydrogel samples were placed in a 6-well plate, treated with 70% ethanol for sterilization, then washed with PBS, and incubated with the growth medium for 30 minutes before use.

2.5.2. Cell viability. The myoblasts were seeded at a density of 2×10^4 cells per well and cultured in growth medium to allow the free spread for 24 hours. The cell viability was visualized by using live/dead staining. Quantification of live cells (green) and dead cells (red) was analyzed by the mean gray value using Fiji software. Three independent samples were analyzed ($n \geq 5$).

$$\text{Cell ratio of live cells (dead cells)} = \frac{\text{number of live cells (dead cells)}}{(\text{number of live cells} + \text{number of dead cells})}$$

2.5.3. Cell proliferation. The myoblasts were seeded at a density of 1×10^4 cells per well and cultured in growth medium overnight to allow the free spreading on the scaffolds. The cells were incubated and tested for 24 and 48 hours. Cell proliferation was measured by the counting cell nuclei number using Fiji software. At the end of the cell culture time point, the cells were washed with PBS and fixed using 3.7% paraformaldehyde for 15 minutes and then the cell membrane was permeabilized with 0.5% Triton X-100 solution for 15 minutes, followed by incubating with DAPI for 1 hour, following with PBS washing in 3 times. Immunofluorescence imaging was done using a fluorescence microscope (Microscope DM4000b). The nuclei number was evaluated using Fiji software. Three independent samples were analyzed ($n \geq 5$).

2.5.4. Cell differentiation. The myoblasts were cultured on the different samples at a density of 4×10^4 cells per well and incubated with growth medium to 100% confluence. Cells were subjected to differentiation medium and observed at 3 and 8 days. For the staining protocol, the cells were fixed using 3.7% paraformaldehyde solution. Afterward, the cell membrane was permeabilized using a 0.5% Triton X-100 solution for 15 minutes and blocked with 5% bovine serum albumin in PBS solution for 30 minutes. The cells were subsequently incubated with the primary antibody for mouse-anti-human Myosin heavy chain (Myosin 4 Monoclonal Antibody, Thermofisher, 1 : 200) in PBS with 1% FBS for 3 hours at 4 °C and then incubated with goat anti-mouse IgG H&L (Alexa Fluor® 488, 1 : 500) in PBS with 1% FBS and DAPI for 1 hour, following with PBS washing in 3 times. The imaging was done using a fluorescence microscope (Microscope DM4000b). The Myotube number, area, diameter and length were evaluated using Fiji software. CellProfiler software evaluated the fusion index and the percentage of total nuclei inside the myotubes. Three independent samples were analyzed ($n \geq 5$).

2.5.5. Statistical analysis. One-way analysis of variance (ANOVA) was used to compare values among different experiment groups using GraphPad Prism 6 software. P value (<0.05) was considered statistically significant: $^*P < 0.05$; $^{**}P < 0.01$. All data were expressed as mean value ± standard deviation of at least triplicate experiments.

3. Results and discussion

3.1. fCNT synthesis and characterization

CNTs were decorated with trimethyl ammonium benzene groups through the diazotization reaction to obtain fCNT, as shown in Fig. 1. The diazotization reaction was performed in water at 80 °C (see Experimental details in section 2.1).[37] The diazonium precursor 4-amino-*N*,*N*,*N*-trimethylbenzene ammonium iodide was obtained through methylation of *N*,*N*-dimethylbenzene-1,4-diamine[38] and activated *in situ* with isopentyl nitrite. The method herein employed for CNT functionalization relies on a synthetic strategy readapted from our previous works[10,37,39] and based on the Tour diazotization reaction.[40] This type of reaction allows the covalent attachment of substituted benzene rings to carbon nanostructures and leads to a good degree of functionalization. The reaction is fast, effective, well-reproducible, free from hazardous reagents or soluble toxic contaminants and, being carried out in water, it does not leave residual organic solvents adsorbed on the nanostructures. Moreover, a proper choice of reaction conditions allows for limited damage to the structure of the basal plane and thus retains the properties of the nanotube, unlike functionalization based on harsh oxidative treatments.

3.1.1. Raman spectroscopy. Raman spectroscopy was performed to test the structural integrity of fCNT after the functionalization treatment. In particular, the typical Raman signals of carbon nanotubes were found at 1332 cm^{-1} for the D band, at 1595 cm^{-1} for the G band and 2654 cm^{-1} for the D* overtone (Fig. S1, ESI†). The relative intensity of the D and G bands could be associated with the changing of carbon hybridization from sp^2 to sp^3 due to the covalent introduction of functional groups and the introduction of structural defects.[41] However, this behaviour is hardly found for CNTs in which only

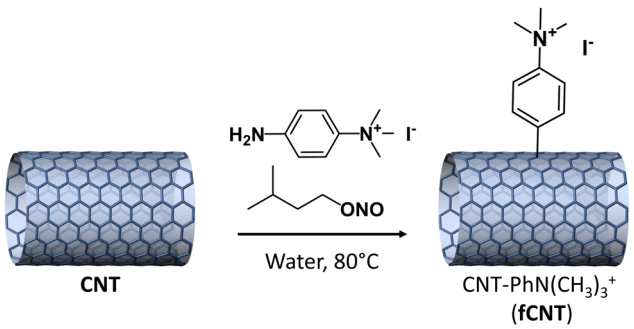

Fig. 1 Reaction scheme of CNT functionalization with 4 amino-*N*,*N*,*N*-trimethylbenzene ammonium iodide through the diazotization reaction.

the outermost layer can be functionalized while the inner layers remain intact. In our case, Raman spectra were recorded at 3 different locations of the samples, and the difference between the D/G ratios in pristine CNTs and fCNT was not statistically significant.

3.1.2. X-ray photoelectron spectroscopy (XPS). XPS measurements were performed to confirm the covalent functionalization of CNTs with trimethylbenzene ammonium groups. Results are reported in Fig. 2 and Table 2. The analysis of the C 1s region of CNTs shows a main peak at 284.1 eV attributed to C sp^2 and a small component at 285.0 eV related to C sp^3. In addition, weak peaks ascribed to oxygenated groups are detected, such as alcoholic (286.0 eV), carbonyl (287.9 eV) and carboxylic (288.9 eV) groups. The C 1s region for fCNT is similar to that for the CNT; however, an increase of the C–N component at 286.0 eV is observed, suggesting the successful functionalization. The analysis of the N 1s region confirms the CNT modification as fCNT showing the expected $(CH_3)_3$–N^+ component at 402.9 eV.[42] In addition, another component at 399.4 eV is observed, which could be attributed to –N=N– moieties.[43] Indeed, azobenzene bonds may form during the functionalization, through diazo coupling of diazonium salts with *N*,*N*,*N*-trimethylbenzene ammonium groups already anchored on the CNT surface, or from the radical splitting of a diazoanhydride formed throughout the radical propagation mechanism proposed for the Tour reaction.[44,45] This result is in agreement with similar evidence already reported for this kind of CNT functionalization.[39] We hypothesized that azo coupling may compete with the reduction of the diazonium salt thus increasing the amount of nitrogen species on the surface and leading to the formation of multiaryl layers on CNTs. On the other hand, it cannot be excluded that a small fraction of the aniline reagent remains adsorbed on CNTs, since the –NH_2 component would overlap with the –N=N– signal (Fig. 2b). However, the difference between the ratios of the two N components for fCNT and for the aniline reagent excludes the hypothesis that all aniline molecules are adsorbed on the CNT surface without reacting. The surface composition of fCNT was obtained from the C 1s, N 1s and O 1s peak regions, taking into account the corresponding sensitivity factors. Accordingly, a nitrogen component of 3.0 at% is introduced by the functionalization process.

Table 2 Analysis of the XPS results. For each sample, the binding energy and the at% of the C 1s components are reported

Sample	C sp^2	C sp^3	C–OH/C–N	Carbonyl groups	Carboxylic groups
CNT	284.1 eV	285.0 eV	286.0	287.5 eV	288.9 eV
	79.1%	8.3%	5.7%	4.3%	2.6%
Fcnt	284.1 eV	285.0 eV	286.0	287.5 eV	288.9 eV
	74.6%	10.2%	11.1%	4.1%	0%

3.1.3. Thermogravimetric analysis (TGA). Thermogravimetric analysis was used to assess the degree of functionalization of fCNT through the thermal decomposition of the material. The analysis was performed between 100 and 1000 °C in a nitrogen atmosphere in both the pristine CNT and fCNT samples to observe the difference in weight percentage due to the introduction of the functional groups, as shown in Fig. 3. In particular, the pristine CNT material did not degrade significantly below 550 °C, whereas fCNT displayed a higher weight loss of 6.2%, which can therefore be attributed to the introduced organic functionalities. From this analysis, an

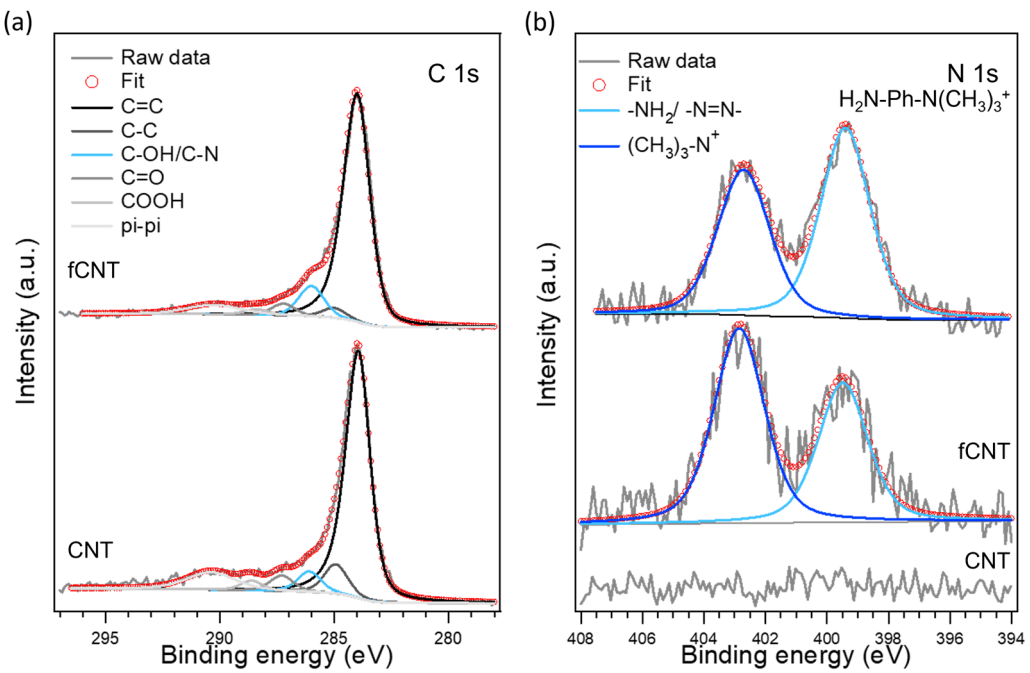

Fig. 2 C 1s and N 1s XPS regions of the pristine (CNT) and functionalized (fCNT) carbon nanotubes. The N 1s spectrum of 4-amino-*N*,*N*,*N*-trimethylbenzene ammonium iodide (H_2N–Ph–$N(CH_3)_3^+$) has been added as reference.

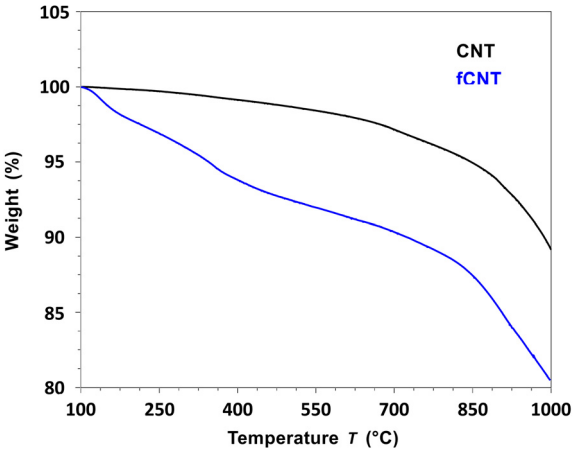

Fig. 3 Overlay of thermograms of pristine CNTs and fCNT recorded from 100 to 1000 °C in a nitrogen atmosphere.

estimation of the functionalization degree (FD) was calculated as the ratio between the number of moles of functional groups and the number of moles of carbon (see details in S1, ESI†). Although the resulting FD is as low as 0.3%, it must be considered that this value is related to the total amount of carbon in the nanostructure, while only the outer wall of the multi-walled CNT can be functionalized, so a low ratio between the number of functional groups and carbon atoms is expected. In fact, the atomic component of nitrogen obtained from XPS is one order of magnitude higher (3.0 at%), since this measurement involves only the outer layers of the material. Since the exact amount of carbon that belongs to the external wall is unknown, the density of functional groups on the surface cannot be unambiguously calculated.

3.1.4. fCNT standard water dispersion characterization. Due to the intrinsically heterogeneous nature of CNT samples (*e.g.* in terms of length, diameter, and degree of aggregation), chemical modification is expected to afford mixtures of CNTs with different degrees of functionalization and solubilities, and the maximum concentration obtained for a solution of CNT derivatives is strongly dependent on the dispersion procedure.[46] Therefore, a standard dispersion of fCNT in water was prepared according to a specific procedure (see Section 2.2.4) allowing the comparison of different CNT derivatives[10] and characterized by dispersibility, DLS and ZP measurements. While pristine CNTs are completely insoluble in water, fCNT formed a stable dispersion of 1.25 mg mL^{-1}. Particle dimensions in water were analyzed *via* DLS using the Stokes–Einstein equation as an approximation for spherical fCNT aggregates.[47] In fact, the DLS provides the average hydrodynamic radius of perfectly spherical objects; thus, in our case, the numerical results cannot be taken as real diameter values, but they can be used as a relative indication of the size of the particles, to compare dispersions of similar nanostructures. The resulting hydrodynamic mean diameter was 138.4 ± 2.5 nm, which is slightly lower than values reported in the literature for other CNT derivatives in water.[48,49] This is in agreement with a reduced aggregation tendency, thanks to the functionalization, thus leading to an average smaller size of the particles. The polydispersity index of the dispersion was 0.250, which is attributed to a moderately polydisperse size distribution. In addition, the ZP value of +43.2 ± 0.8 mV was coherent with a stable dispersion with positive charges, thus supporting a successful functionalization with quaternary ammonium groups.[50]

3.1.5. The positively charged fCNT coordinates with alginate. DLS and ZP were used to confirm the electrostatic interaction between alginate and the positively charged CNT derivative. To this aim, an alginate/fCNT adduct (alginate@fCNT) was prepared by mixing the two compounds in water and then removing the excess alginate through repeated centrifugation/washing steps (see details in Section 2.2.7), thus leaving only those polymer chains that are stuck (or wrapped) on fCNT walls. The obtained solid alginate@fCNT was then redispersed in water and analysed to evaluate the particle size and zeta potential response. These outcomes were compared with a control sample containing only fCNT (different from the standard dispersion), prepared according to the procedure detailed in Section 2.2.7.

A hydrodynamic mean diameter of 291.0 ± 3.6 nm was measured for alginate@fCNT, which falls in the same size range obtained for the fCNT control sample (313.0 ± 9.1 nm), also considering the above-mentioned approximation about the shape of the nanoparticles. This evidence rules out the presence of macroaggregates of alginate chains and confirms the effectiveness of the washing procedure. Once the removal of excess alginate was verified, the interaction between fCNT and alginate was investigated through ZP analysis. The negative ZP value (−36.7 ± 0.4 mV) obtained for alginate@fCNT, compared with the positive potential of fCNT (33.4 ± 0.2 mV), can be ascribed to the alginate carboxylate groups.[51] This indicates that the negatively charged polymer is still wrapping the nanotubes, even after repeated washing steps, thanks to strong interactions with the positively charged fCNT surface. This evidence supports the hypothesis that ammonium groups help to stabilize the dispersion of fCNT in the hydrogel scaffold and prevent migration into the cell environment.

3.2. Scaffold preparation, characterization and cell studies

Since the physical properties of an alginate hydrogel are affected by its specific preparation procedure,[52] we considered two different gelation techniques based on ionic crosslinking with Ca^{2+} ions, in order to test if they give rise to different responses to the inclusion of the fCNT filler, and in turn different cell behaviors (details on scaffold preparation are provided in Section 2.3). Specific preparation conditions were chosen to obtain values of stiffness in the range of 25–90 kPa, which is typically measured for skeletal muscle tissues in murine[53–55] and rabbit.[56]

The external gelation method is based on an external crosslink source and gelation is achieved by the established equilibrium between alginate and $CaCl_2$ solutions, which are physically separated by a dialysis membrane. Usually, this technique leads to the formation of a stiff but not uniform

material. Instead, the internal gelation occurs from inside the hydrogel after homogeneously mixing the alginate solution with a $CaCO_3$ crosslinker solution and an acid component.[57] This method is known to lead to the formation of a soft and highly porous hydrogel due to the evolution of CO_2 from the $CaCO_3$ source during the crosslinking[52] and allows tuning of the mechanical and chemical properties of hydrogels by changing the amount of Ca^{2+} and alginate used.[22,58] Plain alginate hydrogels HG1 and HG2 were obtained through external gelation and internal gelation, respectively. By adding a fCNT dispersion to the alginate solution before gelation, composite hydrogels HG1-fCNT and HG2-fCNT were prepared, with a 0.01 w/v% fCNT loading. This value, much lower than what can be found in the literature,[16,30] was chosen to minimize toxicity. A thorough characterization of the alginate discs was carried out to study the different properties provided by the two gelation methods and by the presence of fCNT. The scaffolds were tested in terms of mechanical, electrical, and cell adhesion properties, promoting myoblast growth and differentiation.

3.2.1. Scaffold ultrastructure and fCNT distribution. The porosity of the samples and the distribution of fCNT in the matrix were assessed by SEM at different magnifications, as shown in Fig. 4. Although it is rather complex to draw clear insights into the hydrogel porosity (*i.e.* the preparation of the samples may have altered their structure by forming ice crystals during freeze-drying), the samples can be compared as they have undergone the same treatment. In general, cross-sections revealed a typical macroporous structure in the range of 10–500 μm with a rather uniform distribution in all samples.[59] However, external and internal gelation techniques resulted in different morphological structures, probably due to the different ways the crosslinker ions get in contact with the alginate chains and the development of CO_2 in the case of HG2-type hydrogels.[60] The structure of HG2 indeed looks very airy, while that of HG1 exhibits wider pores featuring a certain extent of anisotropy. In addition, the presence of a fibrous network with a certain nano porosity is detectable at higher magnification in all samples, but it is particularly pronounced in HG1-type hydrogels. Interestingly, the detection of carbon nanotubes is clearer for the HG2-fCNT sample, where carbon nanotubes are exposed on the surface of the alginate pores. In contrast, carbon nanotubes are hardly recognized within the fibrous matrix of the HG1-fCNT sample.

3.2.2. Scaffolds' mechanical properties. The elastic modulus of the alginate hydrogels was measured for freshly prepared samples. Scaffolds obtained through external gelation gave values of 106.7 ± 5.5 kPa and 67.9 ± 11.4 kPa for HG1 and HG1-fCNT, respectively. Lower values were obtained for samples from internal gelation: 46.6 ± 9.3 kPa and 35.7 ± 13.7 kPa for HG2 and HG2-fCNT respectively. These results are in agreement with the low stiffness usually obtained by the internal gelation method.[22] Interestingly, in both scaffolds, the introduction of fCNT tends to decrease the stiffness of the alginate, probably partially hampering the crosslinking with Ca^{2+} ions.

3.2.3. Scaffolds' behaviour in cell medium. In order to test the stability of the scaffolds, we kept them in a calcium-increased cell culture medium for ten days, which is a typical time frame required for myoblast differentiation. During this period, we monitored the scaffold properties by observing variations in weight, size and stiffness. All samples tend to lose weight in the culture medium, more significantly during the first two days, resulting in a weight loss of 20–30% of the initial weight within 10 days, as shown in Fig. 5a. This is probably due to the diffusion of free water molecules from the material to the culture medium. This trend is associated with the shrinking of hydrogel disks, as visible in the pictures in Fig. 5b, also showing that the structural integrity of the scaffolds is preserved. Indeed, the diameters of these samples decreased by 12.5% in ten days. No significant differences in these trends were found with the addition of carbon nanotubes in the samples, probably due to the low amount of nanostructure used; on the other hand, the two types of alginates exhibited very different mechanical behaviour, as shown in Fig. 5c. The elastic modulus for hydrogels from external gelation exhibited a slight decrease during the initial three days, subsequently returning and remaining stable to approximately 100 kPa for HG1 and 70 kPa for HG1-fCNT from day five. The elastic

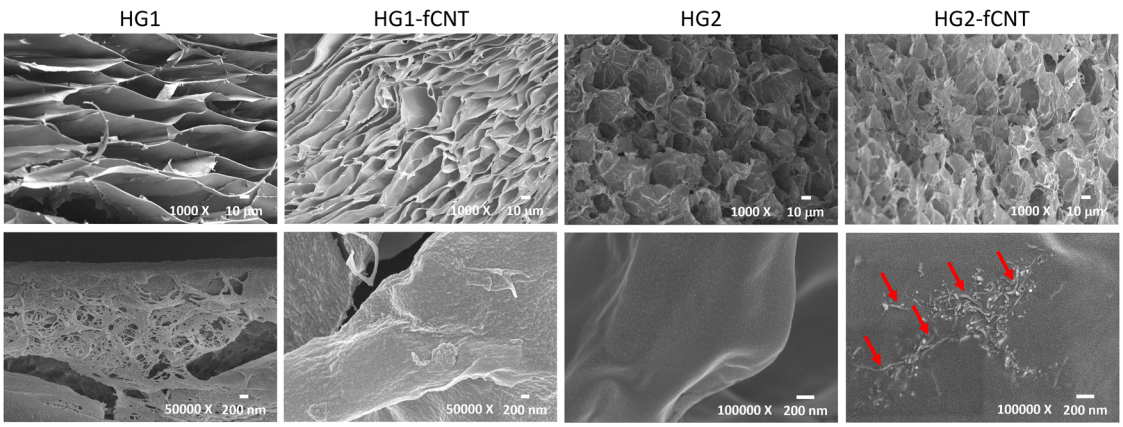

Fig. 4 SEM images of the cross section of alginate scaffolds taken at different magnifications. Arrows point to some of the visible fCNT.

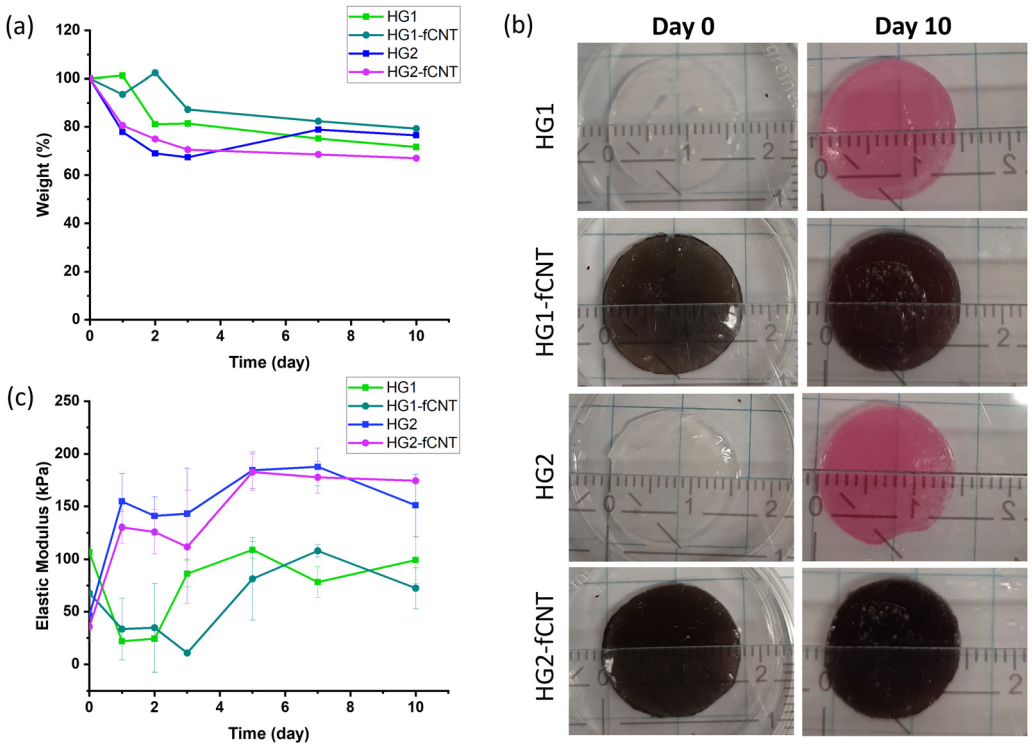

Fig. 5 (a) Weight changes, (b) gross appearance and (c) elastic modulus of hydrogel samples in contact with cell culture medium for ten days.

modulus of samples from internal gelation, conversely, exhibited a rapid increase from the initial days and subsequently stabilised at around 170 kPa for both HG2 and HG2-fCNT from day five. Probably, the tendency of hydrogels from internal gelation to increase stiffness during immersion in the calcium-enhanced medium could be explained by a better ability of Ca^{2+} ions to reach the alginate chains thanks to the larger and more interconnected pores than in hydrogels from external gelation. As a result, additional crosslinking sites are formed in HG2 and HG2-fCNT after soaking. Instead, the stiffness of HG1 and HG1-fCNT hydrogels remained approximatively constant. These samples may have already reached a maximum crosslinking capacity and thus maximum mechanical properties as a consequence of the gelation method employed. However, after a few days, an equilibrium was reached in all hydrogel samples, which then remained stable in terms of weight and mechanical properties.

In this instance, we demonstrated that the simple addition of calcium ions into the cell medium can stabilize the crosslinking network, thereby preventing the degradation of the material, which is often associated with the uncontrolled exchange of divalent ions with the surrounding medium and subsequent dissolution.[19] As reported in the literature, this degradation tendency can be reduced by using different crosslinkers, such as Al^{3+} and Fe^{3+} cations, which bind to alginate more efficiently,[61] polyelectrolyte as linear polyethyleneimine (LPEI),[33] or covalent crosslinkers through carbodiimide chemistry.[62,63] In addition, to overcome these issues, alginate can be coupled with other biomaterials such as cellulose, collagen or hyaluronic acid.[60,64]

3.2.4. Scaffolds' electrical properties. Electrical features of scaffolds play a crucial role in tissue engineering of electroactive tissues.[65,66] A range of different approaches for the electrical characterization of hydrogels are found in the literature, including either AC or DC measurements as well as different electrochemical configurations (*i.e.* 2, 3 and 4 electrodes cells);[67–70] therefore, no standard protocol is available to be used as a benchmark. Since we aim at using hydrogels as scaffolds for 2D cell cultures, where only one surface of the sample is physically in contact with the cells, we chose a measurement setup based on coplanar charge transport with respect to the microelectrodes instead of the bulk transport throughout the hydrogel. More precisely, we cast physically such hydrogels onto IDEs (see more details in Materials and methods, subsection 2.4.4), thereby tracking the ionic and electronic currents that flow coplanar in between the microelectrodes. As previously mentioned, this approach mimics more reliably the cell stimuli onto the hydrogel. Within this context, we performed three types of electrochemical assays: (i) cyclic voltammetry (Fig. 6a and Fig. S4, ESI†), (ii) pulsed measurements (Fig. 6b) and (iii) electrochemical impedance spectroscopy (Fig. 6c and Fig. S6–S8, ESI†), thereby extracting different parameters such as specific capacitance, indicial impedance and comprehensive impedance behaviour as a function of a wide range of frequencies. These parameters allow one to extract relevant information such as the capability of storing charges (*i.e.* specific capacitance), the time-varying resistance related to a step potential (*i.e.* ΔV = 200 mV)[71] and the overall impedimetric behaviour ranging from 10^5 to 10^{-1} Hz. According to the specific capacitance, both pristine hydrogels,

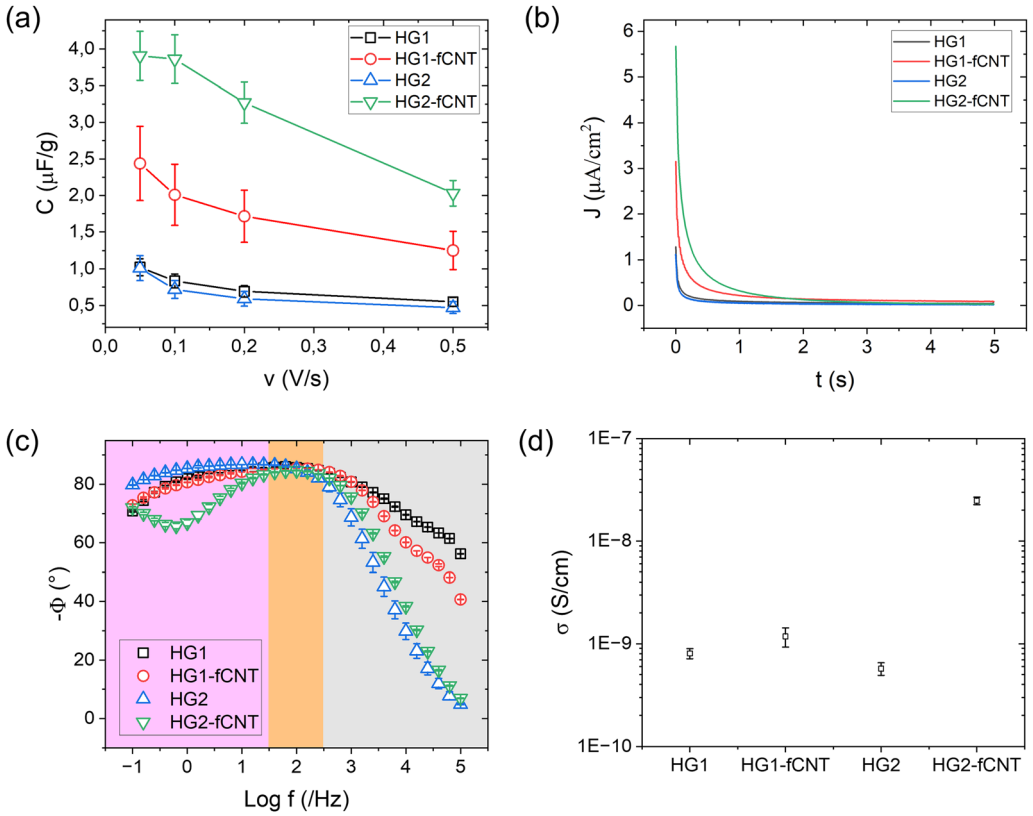

Fig. 6 (a) Overlay of the specific capacitance, (b) pulsed measurements (ΔV = 200 mV) and (c) Bode plot phase trend (EIS) for the 4 hydrogels. Grey, orange and magenta areas highlight the high-, intermediate- and low-frequency regions. (d) Plot of the conductivity for the four hydrogels.

namely HG1 and HG2, show lower values of specific capacitance than the corresponding composites, *i.e.* HG1-fCNT and HG2-fCNT. According to the literature, these values are consistent with other hydrogels based on alginate, whose order of magnitude is similar, namely from 1 to 10 μF cm^{-2}.[69] The highest values of specific capacitance are the ones related to HG2-fCNT, so the internal gelation provides a behavior that would be appealing for applications such as energy storage. Coherently, the pulsed measurements point out a beneficial effect of using fCNT for such hydrogels. As a result, a clear decrease of the indicial impedance is monitored by adding fCNT, in fact 97.5 MΩ cm^{-2} and 40.0 MΩ cm^{-2} for HG1 and HG1-fCNT, whereas 112.5 MΩ cm^{-2} and 22.5 MΩ cm^{-2} for HG2 and HG2-fCNT. Aiming at a more comprehensive view of these 4 hydrogels, EIS provides more precise information since many phenomena can be monitored even though they feature different time constants. It is useful to define three frequency regions: (i) high- (grey region in Fig. 6c), (ii) intermediate- (orange region in Fig. 6c) and (iii) low-frequency-(magenta region in Fig. 6c) regions. The higher frequency region shows the discrepancy between internal gelation and external gelation; in contrast, the lower frequency region highlights the effect of fCNT in the HG2 hydrogel. Finally, hydrogel conductivity (σ) can be extracted by taking into account the resistive elements of the equivalent circuits as well as the geometrical factor of our IDEs. HG1, HG1-fCNT, HG2 and HG2-fCNT show $\sigma_{HG1} = 8.1 \times 10^{-10}$ S cm^{-1}, $\sigma_{HG1\text{-}fCNT} = 1.2 \times 10^{-9}$ S cm^{-1}, $\sigma_{HG2} = 5.7 \times 10^{-10}$ S cm^{-1}, and $\sigma_{HG2\text{-}fCNT} = 2.8 \times 10^{-8}$ S cm^{-1}, respectively (Fig. 6d). Although the values of conductivity are lower than other hydrogels (namely 10^{-3} S cm^{-1}), one must take into account the geometry of the electrochemical cell, and more precisely the contact area of the hydrogel exploited to perform these electrochemical measurements. Aside from this aspect, the addition of fCNT affects dramatically the conductivity of the internal gelation hydrogel; in fact, it increases by more than 1 order of magnitude, which is even coherent to the indicial impedance measured by the pulsed tests. For this reason, HG2-fCNT is the most promising candidate to support the cell stimuli. More interestingly, this hydrogel shows a more pronounced resistive behaviour compared to the other ones in the lower frequency region, whose time scale matches one of the biological tissues, namely from 1 ms to 100 ms.

3.2.5. Cell viability. Cell viability and cytocompatibility of the scaffolds were assessed by live/dead staining, as shown in Fig. 7a. The percentage of living cells was ≥95% for all alginate samples, suggesting that the scaffolds were not cytotoxic for myoblasts, even in the presence of fCNT. In fact, the low fCNT amount used, and the chemical surface functionalization avoid possible cell toxicity issues, often associated with the agglomeration state of pristine nanostructures.[9,72,73] Moreover, differences in cell morphology are visible in Fig. 7b. The myoblasts on both HG1-type samples look nicely attached to the hydrogel surface and display a typical elongated shape. Instead, cells on HG2-type samples behave differently. On HG2, cells tend to show a more rounded shape and form aggregates, while on HG2-fCNT they seem to adhere better, exhibiting a more

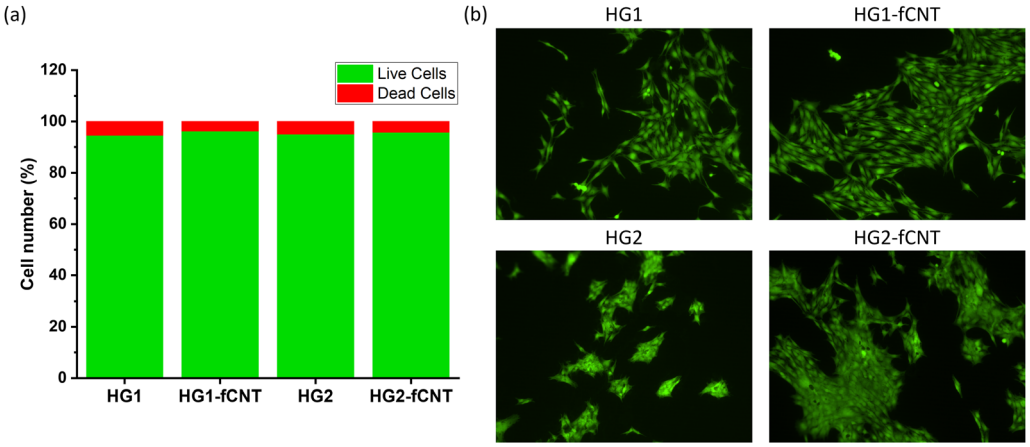

Fig. 7 (a) Cell viability assay and (b) cell morphology through live and dead staining. The scale bar is 100 μm with a magnification of 10×.

stretched shape. This is probably due to the presence of exposed carbon nanotubes that can act as cell adhesion sites on the walls of alginate pores. Indeed, alginates are known to exhibit poor cell adhesion,[74] while the presence of carbon nanotubes in the hydrogels has already been reported to enhance cell adhesion *in vitro*.[16,30] Typically, alginates could also be modified with short amino acid sequences found in the ECM such as collagen, laminin, or fibronectin-derived adhesion peptide arginine glycine aspartic acid (RGD) in order to be used for cell studies.[75–77] Another decisive factor affecting cell adhesion is stiffness;[78] in fact, scaffolds with too low elastic modulus may not guarantee the elongation of cells on the

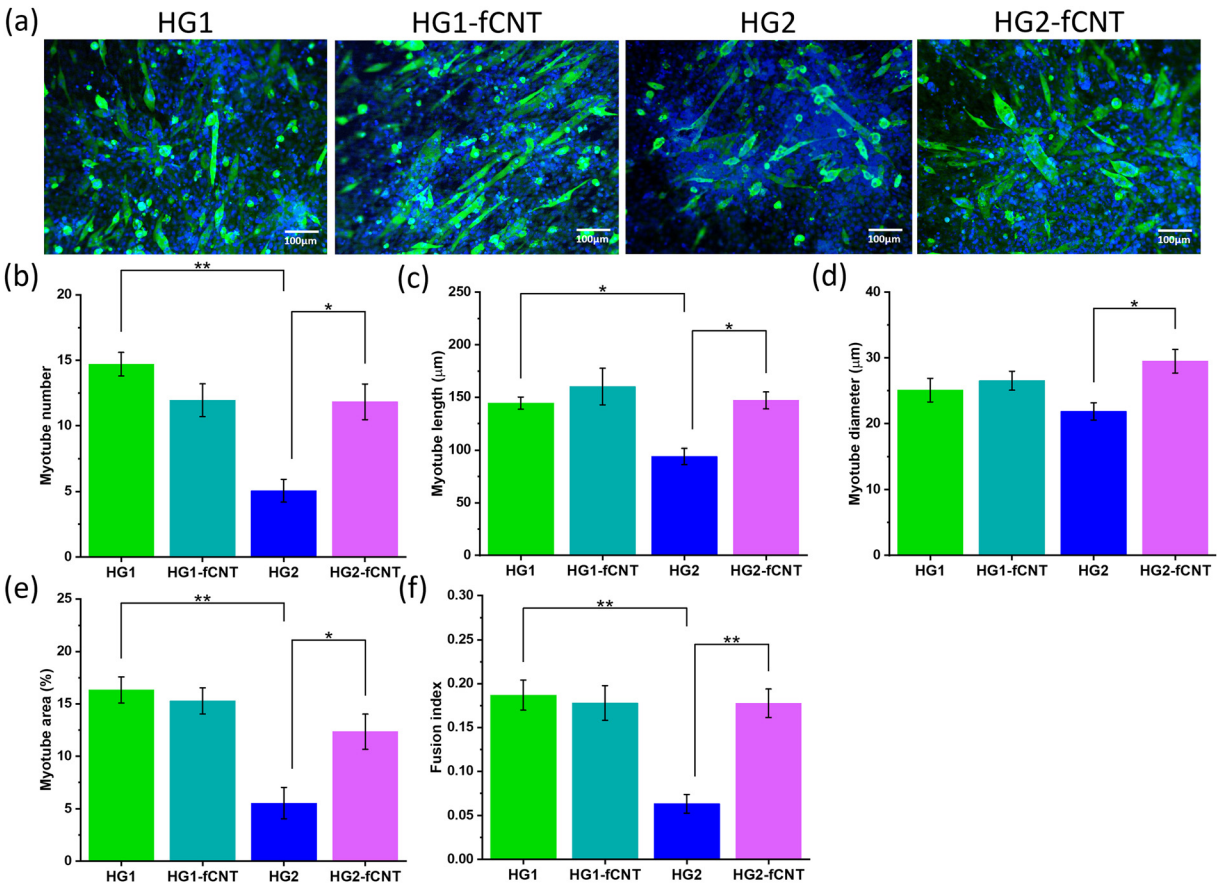

Fig. 8 (a) Myoblast differentiation and myotube formation after 8 days. The scale bar is 100 μm. (b) Myotube number, (c) length, (d) diameter, (e) area, and (f) fusion index in the alginate samples, obtained through data analysis of cell differentiation images. The statistical test used is one-way analysis of variance (ANOVA). Data are shown as mean ± standard deviation (SD) of triplicate experiments (n = at least 50 myotubes, $^{*}P < 0.05$, $^{**}P < 0.01$). P value < 0.05 is considered statistically significant.

surface. This might explain the difference in cell adhesion between HG1 and HG2. Indeed, HG1 showed a higher elastic modulus value at the beginning of the cell culture.

3.2.6. Cell proliferation and differentiation. Myoblasts were seeded on hydrogel scaffolds and proliferation and differentiation were checked within 2 and 8 days, respectively. Results on cell proliferation displayed no significant differences between the samples (Fig. S3, ESI†). Contrary to what has been reported in the literature, in this case fCNT did not provide a clear improvement in cell responses.[16,30,79] However, the most striking results emerge from the differentiation studies. After two days of proliferation, myoblasts start to fuse into multinucleated myofibrils and form myotubes.[80] Specifically, myoblasts differentiated into myotubes in all samples, as shown in Fig. 8a, but a significant difference was found between the two types of alginate hydrogels in the number and morphology of the myotubes. To better clarify the outcomes, a thorough analysis of the data was performed by calculating the myotube number, length, diameter, area percentage, and fusion index, as shown in Fig. 8b–f, respectively. Data analysis demonstrated that both HG1 and HG1-fCNT had good cell differentiation abilities in all parameters analysed; however, no improvement resulted from the presence of fCNT. On the other hand, the HG2 sample displayed a worse fusion index and number, length and area of myotubes than HG1, which means it was not very suitable for myoblast differentiation. However, the presence of the positively charged fCNT improved all the parameters studied for the material, especially the fusion index.

The differences between bare HG2 and HG2-fCNT observed in cell adhesion and differentiation could be explained, as already mentioned, by the exposure of fCNT particles on the hydrogel surface, acting as adhesion sites, but also by the difference in electrical behaviour detectable precisely at low frequencies, in the range of bioelectrical signalling. We already demonstrated that the dispersion of CNT derivatives in non-conductive biomaterials can improve the interaction with cells, helping the differentiation in electroactive tissues.[10,32] Specifically, the literature reported several examples supporting the hypothesis that electrical conductivity at low frequencies could be beneficial for cell growth and differentiation.[65,67,70] Moreover, the presence of CNTs in alginate hydrogels probably enhances the very first cell adhesion onto these substrates, consequently affecting cell fate.[16,30] On the other hand, HG1 was not affected by the presence of fCNT; this could be because carbon nanotubes were not exposed on the surface of the material; therefore, they were not directly in contact with the cells, and the surface electrical conductivity of HG1 and HG1-fCNT was the same at low frequencies. Another explanation for this peculiar behavior could be that both HG1 and HG1-fCNT showed a mechanical stiffness of about 100 kPa with little fluctuation over a period of ten days. This stiffness value is very close to that of the skeletal muscle tissue of 25–90 kPa, indicating that the samples probably had the best mechanical properties for myoblast growth. In fact, stiffness is one of the most important factors for cell growth and differentiation. If modulated properly, it can adapt to the mechanical properties of the tissue of interest and help cells to attach and grow well on the scaffold.[81] Indeed, both HG1-type hydrogels displayed better cell adhesion than HG2 already in the first 24 hour, and this may have influenced cell fate also in terms of differentiation.

4. Conclusions

CNTs were successfully functionalized with positively charged trimethyl ammonium benzene groups affording fCNT derivatives with good dispersibility in water. The soluble CNT derivatives were homogeneously dispersed in alginate-based hydrogels obtained through two different gelation methods (external gelation for the HG1 series, by addition of $CaCl_2$, and internal gelation for the HG2 series, based on $CaCO_3$).

The physical properties of the resulting materials, either with or without CNT fillers, were compared and correlated with the effects on myoblast growth and differentiation. It was shown that the gelation routes significantly influenced relevant features such as pore morphology and stiffness, while the addition of fCNT lowered the elastic modulus in both matrices. A thorough electrical characterization was carried out through a methodology and a setup that we have specifically designed for our hydrogel scaffolds. This allowed us to highlight that, while the native electrical properties of the two kinds of hydrogels are very similar, the inclusion of fCNT has a prominent effect on HG2. Indeed, HG2-fCNT, besides showing a higher conductivity, transmitted low frequency signals (typical of electroactive biological tissues) at a higher rate compared to the other examined scaffolds.

The proposed functionalization of CNTs allowed us to obtain composite scaffolds fulfilling cell viability and cytocompatibility with both gelation methods. Interestingly, the addition of fCNT had a more relevant effect on the scaffold obtained through internal gelation. Precisely, in HG2-fCNT, where the nanotubes provide a significant improvement in electrical properties, there is also an enhancement in cell differentiation. We can therefore conclude that HG2-fCNT is the most promising scaffold for tissue engineering applications, considering not only the observed effect on cells but also its potential advantage in active electrical stimulation. Noteworthy, the observed effects were obtained with a very low loading of fCNT, thanks to the specific functionalization strategy.

Further steps towards the use of such hybrid scaffolds may explore strategies to achieve an aligned topography on the surface to further promote myoblast differentiation into myotubes. The addition of proteins and growth factors within the hydrogel is also an option to stimulate cells and recreate an improved biomimetic environment.[82,83] Moreover, testing our scaffold also on different cell lines responding to electric stimuli, such as neurons, may lead to similar or even more interesting results.

Data availability

The data supporting this article have been included as part of the ESI.†

Conflicts of interest

The authors declare the following financial interests/personal relationships which may be considered as potential competing interests: Patrick van Rijn reports a relationship with BiomACS BV that includes equity or stocks, being the co-founder, scientific advisor, and share-holder of BiomACS BV, a biomedical oriented screening company. The authors declare no other competing interests.

Acknowledgements

Financial support from the University of Padova is acknowledged by EM, LCa for grant P-DiSC#05BIRD2021-UNIPD (CORDER) and by SC for grant P-DiSC#11NexuS_BIRD2020-UNIPD (CARBON-FET). The PhD fellowship of L.Ce. was financed by PON 2014-2020 (National Operative Program 'Research and Innovation') D.M. n. 1061, August 10th 2021, Action IV.5. The PhD fellowship of T. F. was financed by the Chinese Scholarship Council (No. 202106170045).

References

1 A. S. Mao and D. J. Mooney, Regenerative Medicine: Current Therapies and Future Directions, *Proc. Natl. Acad. Sci. U. S. A.*, 2015, **112**(47), 14452–14459, DOI: **10.1073/pnas.1508520112**.

2 M. I. Echeverria Molina, K. G. Malollari and K. Komvopoulos, Design Challenges in Polymeric Scaffolds for Tissue Engineering, *Front. Bioeng. Biotechnol.*, 2021, **9**, 617141, DOI: **10.3389/fbioe.2021.617141**.

3 C. M. Murphy and F. J. O'Brien, Understanding the Effect of Mean Pore Size on Cell Activity in Collagen-Glycosaminoglycan Scaffolds, *Cell Adhes. Migr.*, 2010, **4**(3), 377–381, DOI: **10.4161/cam.4.3.11747**.

4 P. Zarrintaj, S. Manouchehri, Z. Ahmadi, M. R. Saeb, A. M. Urbanska, D. L. Kaplan and M. Mozafari, Agarose-Based Biomaterials for Tissue Engineering, *Carbohydr. Polym.*, 2018, **187**, 66–84, DOI: **10.1016/j.carbpol.2018.01.060**.

5 X. Lu, W. Zhang, C. Wang, T.-C. Wen and Y. Wei, One-Dimensional Conducting Polymer Nanocomposites: Synthesis, Properties and Applications, *Prog. Polym. Sci.*, 2011, **36**(5), 671–712, DOI: **10.1016/j.progpolymsci.2010.07.010**.

6 C. Cha, S. R. Shin, N. Annabi, M. R. Dokmeci and A. Khademhosseini, Carbon-Based Nanomaterials: Multifunctional Materials for Biomedical Engineering, *ACS Nano*, 2013, **7**(4), 2891–2897, DOI: **10.1021/nn401196a**.

7 M. Barrejón, S. Marchesan, N. Alegret and M. Prato, Carbon Nanotubes for Cardiac Tissue Regeneration: State of the Art and Perspectives, *Carbon*, 2021, **184**, 641–650.

8 E. L. Hopley, S. Salmasi, D. M. Kalaskar and A. M. Seifalian, Carbon Nanotubes Leading the Way Forward in New Generation 3D Tissue Engineering, *Biotechnol. Adv.*, 2014, **32**(5), 1000–1014, DOI: **10.1016/j.biotechadv.2014.05.003**.

9 N. Vicentini, T. Gatti, M. Salerno, Y. S. H. Gomez, M. Bellon, S. Gallio, C. Marega, F. Filippini and E. Menna, Effect of Different Functionalized Carbon Nanostructures as Fillers on the Physical Properties of Biocompatible Poly (l-Lactic Acid) Composites, *Mater. Chem. Phys.*, 2018, **214**, 265–276.

10 E. Stocco, S. Barbon, L. Ceroni, M. Confalonieri, G. Pulzato, S. Pressi, A. D'Osualdo, M. Contran, R. Boscolo-Berto, C. Tiengo, S. Todros, P. G. Pavan, V. Macchi, R. De Caro, L. Calvillo, E. Menna and A. Porzionato, Partially Oxidized Polyvinyl Alcohol + Functionalized Water Soluble Multiwalled Carbon Nanotubes: A New Conductive Nanocomposite Material with Promising Implications for Neuroregeneration, *J. Sci. Adv. Mater. Devices*, 2024, **9**(3), 100762, DOI: **10.1016/j.jsamd.2024.100762**.

11 G. Suarato, S. Pressi, E. Menna, M. Ruben, E. M. Petrini, A. Barberis, D. Miele, G. Sandri, M. Salerno, A. Schirato, A. Alabastri, A. Athanassiou, R. Proietti Zaccaria and E. L. Papadopoulou, Modified Carbon Nanotubes Favor Fibroblast Growth by Tuning the Cell Membrane Potential, *ACS Appl. Mater. Interfaces*, 2024, **16**(3), 3093–3105, DOI: **10.1021/acsami.3c14527**.

12 L. P. Zanello, B. Zhao, H. Hu and R. C. Haddon, Bone Cell Proliferation on Carbon Nanotubes, *Nano Lett.*, 2006, **6**(3), 562–567, DOI: **10.1021/nl051861e**.

13 G. Scapin, P. Salice, S. Tescari, E. Menna, V. De Filippis and F. Filippini, Enhanced Neuronal Cell Differentiation Combining Biomimetic Peptides and a Carbon Nanotube-Polymer Scaffold, *Nanomedicine*, 2015, **11**(3), 621–632.

14 A. Fabbro, M. Prato and L. Ballerini, Carbon Nanotubes in Neuroregeneration and Repair, *Adv. Drug Delivery Rev.*, 2013, **65**(15), 2034–2044, DOI: **10.1016/j.addr.2013.07.002**.

15 S. Ahadian, J. Ramón-Azcón, M. Estili, X. Liang, S. Ostrovidov, H. Shiku, M. Ramalingam, K. Nakajima, Y. Sakka, H. Bae, T. Matsue and A. Khademhosseini, Hybrid Hydrogels Containing Vertically Aligned Carbon Nanotubes with Anisotropic Electrical Conductivity for Muscle Myofiber Fabrication, *Sci. Rep.*, 2014, **4**(1), 4271, DOI: **10.1038/srep04271**.

16 E. D. Yildirim, X. Yin, K. Nair and W. Sun, Fabrication, Characterization, and Biocompatibility of Single-walled Carbon Nanotube-reinforced Alginate Composite Scaffolds Manufactured Using Freeform Fabrication Technique, *J. Biomed. Mater. Res., Part B*, 2008, **87B**(2), 406–414, DOI: **10.1002/jbm.b.31118**.

17 P. E. Kosnik; R. G. Dennis and H. H. Vandenburgh, Tissue Engineering Skeletal Muscle, *Functional tissue engineering*, Springer, 2003, pp. 377–392.

18 I. M. El-Sherbiny and M. H. Yacoub, Hydrogel Scaffolds for Tissue Engineering: Progress and Challenges, *Glob. Cardiol. Sci. Pract.*, 2013, **3**, 38, DOI: **10.5339/gcsp.2013.38**.

19 K. Y. Lee and D. J. Mooney, Hydrogels for Tissue Engineering, *Chem. Rev.*, 2001, **101**(7), 1869–1880, DOI: **10.1021/cr000108x**.

20 A. D. Augst, H. J. Kong and D. J. Mooney, Alginate Hydrogels as Biomaterials, *Macromol. Biosci.*, 2006, **6**(8), 623–633.

21 K. Joyce, G. T. Fabra, Y. Bozkurt and A. Pandit, Bioactive Potential of Natural Biomaterials: Identification, Retention and Assessment of Biological Properties, *Signal Transduct. Target. Ther.*, 2021, **6**(1), 122, DOI: **10.1038/s41392-021-00512-8**.

22 E. A. Growney Kalaf, R. Flores, J. G. Bledsoe and S. A. Sell, Characterization of Slow-Gelling Alginate Hydrogels for Intervertebral Disc Tissue-Engineering Applications, *Mater. Sci. Eng., C*, 2016, **63**, 198–210, DOI: 10.1016/j.msec.2016.02.067.
23 H.-J. Kong, K. Y. Lee and D. J. Mooney, Decoupling the Dependence of Rheological/Mechanical Properties of Hydrogels from Solids Concentration, *Polymer*, 2002, **43**(23), 6239–6246.
24 C. K. Kuo and P. X. Ma, Ionically Crosslinked Alginate Hydrogels as Scaffolds for Tissue Engineering: Part 1. Structure, Gelation Rate and Mechanical Properties, *Biomaterials*, 2001, **22**(6), 511–521.
25 M. M. Stevens, R. P. Marini, D. Schaefer, J. Aronson, R. Langer and V. P. Shastri, *In Vivo* Engineering of Organs: The Bone Bioreactor, *Proc. Natl. Acad. Sci. U. S. A.*, 2005, **102**(32), 11450–11455, DOI: 10.1073/pnas.0504705102.
26 S. C. N. Chang, J. A. Rowley, G. Tobias, N. G. Genes, A. K. Roy, D. J. Mooney, C. A. Vacanti and L. J. Bonassar, Injection Molding of Chondrocyte/Alginate Constructs in the Shape of Facial Implants, *J. Biomed. Mater. Res.*, 2001, **55**((4)), 503–511.
27 M. Stevens, A Rapid-Curing Alginate Gel System: Utility in Periosteum-Derived Cartilage Tissue Engineering, *Biomaterials*, 2004, **25**(5), 887–894, DOI: 10.1016/j.biomaterials.2003.07.002.
28 A. Patel, S. Mukundan, W. Wang, A. Karumuri, V. Sant, S. M. Mukhopadhyay and S. Sant, Carbon-Based Hierarchical Scaffolds for Myoblast Differentiation: Synergy between Nano-Functionalization and Alignment, *Acta Biomater.*, 2016, **32**, 77–88, DOI: 10.1016/j.actbio.2016.01.004.
29 N. Karousis, N. Tagmatarchis and D. Tasis, Current Progress on the Chemical Modification of Carbon Nanotubes, *Chem. Rev.*, 2010, **110**(9), 5366–5397, DOI: 10.1021/cr100018g.
30 B. Joddar, E. Garcia, A. Casas and C. M. Stewart, Development of Functionalized Multi-Walled Carbon-Nanotube-Based Alginate Hydrogels for Enabling Biomimetic Technologies, *Sci. Rep.*, 2016, **6**(1), 32456, DOI: 10.1038/srep32456.
31 H. J. Johnston, G. R. Hutchison, F. M. Christensen, S. Peters, S. Hankin, K. Aschberger and V. Stone, A Critical Review of the Biological Mechanisms Underlying the in Vivo and in Vitro Toxicity of Carbon Nanotubes: The Contribution of Physico-Chemical Characteristics, *Nanotoxicology*, 2010, **4**(2), 207–246.
32 N. Vicentini, T. Gatti, P. Salice, G. Scapin, C. Marega, F. Filippini and E. Menna, Covalent Functionalization Enables Good Dispersion and Anisotropic Orientation of Multi-Walled Carbon Nanotubes in a Poly(l-Lactic Acid) Electrospun Nanofibrous Matrix Boosting Neuronal Differentiation, *Carbon*, 2015, **95**, 725–730, DOI: 10.1016/j.carbon.2015.08.094.
33 P. T. Kühn, T. L. Meijer, I. Schiavon, M. Van Poll, J. Van Aken, S. Groen, R. Kuijer, T. G. Van Kooten and P. Van Rijn, Non-Covalently Stabilized Alginate Hydrogels as Functional Cell Scaffold Material, *Macromol. Biosci.*, 2016, **16**(11), 1693–1702, DOI: 10.1002/mabi.201600214.
34 P. Sharma, H. Busscher, T. Terwee, S. Koopmans and T. van Kooten, A Comparative Study on the Viscoelastic Properties of Human and Animal Lenses, *Exp. Eye Res.*, 2011, **93**(5), 681–688.
35 A. M. Almonacid Suarez, M. G. L. Brinker, L. A. Brouwer, I. Van Der Ham, M. C. Harmsen and P. Van Rijn, Topography-Mediated Myotube and Endothelial Alignment, Differentiation, and Extracellular Matrix Organization for Skeletal Muscle Engineering, *Polymers*, 2020, **12**(9), 1948, DOI: 10.3390/polym12091948.
36 A. M. Almonacid Suarez, Q. Zhou, P. van Rijn and M. C. Harmsen, Directional Topography Gradients Drive Optimum Alignment and Differentiation of Human Myoblasts, *J. Tissue Eng. Regen. Med.*, 2019, **13**(12), 2234–2245.
37 L. Ceroni, S. Benazzato, S. Pressi, L. Calvillo, E. Marotta and E. Menna, Enhanced Adsorption of Methylene Blue Dye on Functionalized Multi-Walled Carbon Nanotubes, *Nanomaterials*, 2024, **14**(6), 522, DOI: 10.3390/nano14060522.
38 C. Hadad, X. Ke, M. Carraro, A. Sartorel, C. Bittencourt, G. Van Tendeloo, M. Bonchio, M. Quintana and M. Prato, Positive Graphene by Chemical Design: Tuning Supramolecular Strategies for Functional Surfaces, *Chem. Commun.*, 2014, **50**(7), 885–887, DOI: 10.1039/C3CC47056C.
39 P. Salice, E. Fabris, C. Sartorio, D. Fenaroli, V. Figà, M. P. Casaletto, S. Cataldo, B. Pignataro and E. Menna, An Insight into the Functionalisation of Carbon Nanotubes by Diazonium Chemistry: Towards a Controlled Decoration, *Carbon*, 2014, **74**, 73–82, DOI: 10.1016/j.carbon.2014.02.084.
40 J. L. Bahr, J. Yang, D. V. Kosynkin, M. J. Bronikowski, R. E. Smalley and J. M. Tour, Functionalization of Carbon Nanotubes by Electrochemical Reduction of Aryl Diazonium Salts: A Bucky Paper Electrode, *J. Am. Chem. Soc.*, 2001, **123**(27), 6536–6542, DOI: 10.1021/ja010462s.
41 S. Osswald, M. Havel and Y. Gogotsi, Monitoring Oxidation of Multiwalled Carbon Nanotubes by Raman Spectroscopy, *J. Raman Spectrosc.*, 2007, **38**(6), 728–736, DOI: 10.1002/jrs.1686.
42 W. Cao, Z. Wang, Q. Zeng and C. Shen, 13C NMR and XPS Characterization of Anion Adsorbent with Quaternary Ammonium Groups Prepared from Rice Straw, Corn Stalk and Sugarcane Bagasse, *Appl. Surf. Sci.*, 2016, **389**, 404–410, DOI: 10.1016/j.apsusc.2016.07.095.
43 P. Brant and R. D. Feltham, X-Ray Photoelectron Spectra of Aryldiazo Derivatives of Transition Metals, *J. Organomet. Chem.*, 1976, **120**(3), C53–C57.
44 M. E. Lipińska, S. L. H. Rebelo, M. F. R. Pereira, J. A. N. F. Gomes, C. Freire and J. L. Figueiredo, New Insights into the Functionalization of Multi-Walled Carbon Nanotubes with Aniline Derivatives, *Carbon*, 2012, **50**(9), 3280–3294, DOI: 10.1016/j.carbon.2011.12.018.
45 Z. Salmi, S. Gam-Derouich, S. Mahouche-Chergui, M. Turmine and M. Chehimi, On the Interfacial Chemistry of Aryl Diazonium Compounds in Polymer Science, *Chem. Pap.*, 2012, **66**(5), 369–391.
46 P. Salice, P. Maity, E. Rossi, T. Carofiglio, E. Menna and M. Maggini, The Continuous-Flow Cycloaddition of Azomethine Ylides to Carbon Nanotubes, *Chem. Commun.*, 2011, **47**(32), 9092, DOI: 10.1039/c1cc13155a.

47 S. Bhattacharjee, DLS and Zeta Potential – What They Are and What They Are Not?, *J. Controlled Release*, 2016, **235**, 337–351, DOI: **10.1016/j.jconrel.2016.06.017**.

48 Y. Wei, X. Ling, L. Zou, D. Lai, H. Lu and Y. Xu, A Facile Approach toward Preparation of Sulfonated Multi-Walled Carbon Nanotubes and Their Dispersibility in Various Solvents, *Colloids Surf. Physicochem. Eng. Asp.*, 2015, **482**, 507–513, DOI: **10.1016/j.colsurfa.2015.07.005**.

49 H. Liu, J. Wang, J. Wang and S. Cui, Sulfonitric Treatment of Multiwalled Carbon Nanotubes and Their Dispersibility in Water, *Materials*, 2018, **11**(12), 2442, DOI: **10.3390/ma11122442**.

50 R. Li, X. Wang, Z. Ji, B. Sun, H. Zhang, C. H. Chang, S. Lin, H. Meng, Y.-P. Liao, M. Wang, Z. Li, A. A. Hwang, T.-B. Song, R. Xu, Y. Yang, J. I. Zink, A. E. Nel and T. Xia, Surface Charge and Cellular Processing of Covalently Functionalized Multiwall Carbon Nanotubes Determine Pulmonary Toxicity, *ACS Nano*, 2013, **7**(3), 2352–2368, DOI: **10.1021/nn305567s**.

51 G. Khachatryan, K. Khachatryan, J. Szczepankowska, M. Krzan and M. Krystyjan, Design of Carbon Nanocomposites Based on Sodium Alginate/Chitosan Reinforced with Graphene Oxide and Carbon Nanotubes, *Polymers*, 2023, **15**(4), 925, DOI: **10.3390/polym15040925**.

52 X. Liu, W. Yu, Y. Zhang, W. Xue, W. Yu, Y. Xiong, X. Ma, Y. Chen and Q. Yuan, Characterization of Structure and Diffusion Behaviour of Ca-Alginate Beads Prepared with External or Internal Calcium Sources, *J. Microencapsulation*, 2002, **19**(6), 775–782, DOI: **10.1080/0265204021000022743**.

53 A. B. Mathur, A. M. Collinsworth, W. M. Reichert, W. E. Kraus and G. A. Truskey, Endothelial, Cardiac Muscle and Skeletal Muscle Exhibit Different Viscous and Elastic Properties as Determined by Atomic Force Microscopy, *J. Biomech.*, 2001, **34**(12), 1545–1553.

54 I. V. Ogneva, D. V. Lebedev and B. S. Shenkman, Transversal Stiffness and Young's Modulus of Single Fibers from Rat Soleus Muscle Probed by Atomic Force Microscopy, *Biophys. J.*, 2010, **98**(3), 418–424.

55 E. Defranchi, E. Bonaccurso, M. Tedesco, M. Canato, E. Pavan, R. Raiteri and C. Reggiani, Imaging and Elasticity Measurements of the Sarcolemma of Fully Differentiated Skeletal Muscle Fibres, *Microsc. Res. Tech.*, 2005, **67**(1), 27–35, DOI: **10.1002/jemt.20177**.

56 Y. Yoshikawa, T. Yasuike, A. Yagi and T. Yamada, Transverse Elasticity of Myofibrils of Rabbit Skeletal Muscle Studied by Atomic Force Microscopy, *Biochem. Biophys. Res. Commun.*, 1999, **256**(1), 13–19, DOI: **10.1006/bbrc.1999.0279**.

57 C. K. Kuo and P. X. Ma, Ionically Crosslinked Alginate Hydrogels as Sca!Olds for Tissue Engineering: Part 1. Structure, Gelation Rate and Mechanical Properties, *Biomaterials*, 2001, **22**, 511–521, DOI: **10.1016/S0142-9612(00)00201-5**.

58 A. S. Sergeeva, D. A. Gorin and D. V. Volodkin, In-Situ Assembly of Ca–Alginate Gels with Controlled Pore Loading/Release Capability, *Langmuir*, 2015, **31**(39), 10813–10821, DOI: **10.1021/acs.langmuir.5b01529**.

59 A. Sergeeva, A. S. Vikulina and D. Volodkin, Porous Alginate Scaffolds Assembled Using Vaterite CaCO3 Crystals, *Micromachines*, 2019, **10**(6), 357, DOI: **10.3390/mi10060357**.

60 H. Yan, D. Huang, X. Chen, H. Liu, Y. Feng, Z. Zhao, Z. Dai, X. Zhang and Q. Lin, A Novel and Homogeneous Scaffold Material: Preparation and Evaluation of Alginate/Bacterial Cellulose Nanocrystals/Collagen Composite Hydrogel for Tissue Engineering, *Polym. Bull.*, 2018, **75**(3), 985–1000, DOI: **10.1007/s00289-017-2077-0**.

61 C. H. Yang, M. X. Wang, H. Haider, J. H. Yang, J.-Y. Sun, Y. M. Chen, J. Zhou and Z. Suo, Strengthening Alginate/Polyacrylamide Hydrogels Using Various Multivalent Cations, *ACS Appl. Mater. Interfaces*, 2013, **5**(21), 10418–10422, DOI: **10.1021/am403966x**.

62 Z. Salmi, S. Gam-Derouich, S. Mahouche-Chergui, M. Turmine and M. Chehimi, On the Interfacial Chemistry of Aryl Diazonium Compounds in Polymer Science, *Chem. Pap.*, 2012, **66**(5), 369–391, DOI: **10.2478/s11696-012-0135-5**.

63 P. Eiselt, K. Y. Lee and D. J. Mooney, Rigidity of Two-Component Hydrogels Prepared from Alginate and Poly(Ethylene Glycol)−Diamines, *Macromolecules*, 1999, **32**(17), 5561–5566, DOI: **10.1021/ma990514m**.

64 A. Magnani, R. Rappuoli, S. Lamponi and R. Barbucci, Novel Polysaccharide Hydrogels: Characterization and Properties, *Polym. Adv. Technol.*, 2000, **11**(8–12), 488–495.

65 M. Mehrali, A. Thakur, C. P. Pennisi, S. Talebian, A. Arpanaei, M. Nikkhah and A. Dolatshahi-Pirouz, Nanoreinforced Hydrogels for Tissue Engineering: Biomaterials That Are Compatible with Load-Bearing and Electroactive Tissues, *Adv. Mater.*, 2017, **29**(8), 1603612.

66 S. Marchesan, S. Bosi, A. Alshatwi and M. Prato, Carbon Nanotubes for Organ Regeneration: An Electrifying Performance, *Nano Today*, 2016, **11**(4), 398–401.

67 J. Ramón-Azcón, S. Ahadian, M. Estili, X. Liang, S. Ostrovidov, H. Kaji, H. Shiku, M. Ramalingam, K. Nakajima and Y. Sakka, *et al.*, Dielectrophoretically Aligned Carbon Nanotubes to Control Electrical and Mechanical Properties of Hydrogels to Fabricate Contractile Muscle Myofibers, *Adv. Mater.*, 2013, **25**(29), 4028–4034.

68 S. Seifi, A. Shamloo, A. K. Barzoki, M. A. Bakhtiari, S. Zare, F. Cheraghi and A. Peyrovan, Engineering Biomimetic Scaffolds for Bone Regeneration: Chitosan/Alginate/Polyvinyl Alcohol-Based Double-Network Hydrogels with Carbon Nanomaterials, *Carbohydr. Polym.*, 2024, **339**, 122232.

69 A. Raslan, J. Ciriza, A. Ochoa de Retana, M. Sanjuán, M. Toprak, P. Galvez-Martin, L. Saenz-del-Burgo and J. Pedraz, Modulation of Conductivity of Alginate Hydrogels Containing Reduced Graphene Oxide through the Addition of Proteins, *Pharmaceutics*, 2021, **13**, 1473.

70 R. Tutar, Preparation and Characterization of Conductive and Multi-Network Nanocomposite Hydrogels as Potential Scaffolds for Electroactive Tissues, *New J. Chem.*, 2024, **48**, 14736–14745, DOI: **10.1039/D4NJ01930J**.

71 J. R. Macdonald, W. B. Johnson, I. Raistrick, D. Franceschetti, N. Wagner, M. McKubre, D. Macdonald, B. Sayers, N. Bonanos and B. Steele,*et al.*, *Impedance Spectroscopy: Theory, Experiment, and Applications*, John Wiley & Sons, 2018.

72 L. Li, S. Qin, J. Peng, A. Chen, Y. Nie, T. Liu and K. Song, Engineering Gelatin-Based Alginate/Carbon Nanotubes

Blend Bioink for Direct 3D Printing of Vessel Constructs, *Int. J. Biol. Macromol.*, 2020, **145**, 262–271, DOI: **10.1016/j.ijbiomac.2019.12.174**.

73 M. A. Saleemi, M. Hosseini Fouladi, P. V. C. Yong, K. Chinna, N. K. Palanisamy and E. H. Wong, Toxicity of Carbon Nanotubes: Molecular Mechanisms, Signaling Cascades, and Remedies in Biomedical Applications, *Chem. Res. Toxicol.*, 2021, **34**(1), 24–46, DOI: **10.1021/acs.chemrestox.0c00172**.

74 K. Smetanajr, Cell Biology of Hydrogels, *Biomaterials*, 1993, **14**(14), 1046–1050, DOI: **10.1016/0142-9612(93)90203-E**.

75 J. A. Rowley, G. Madlambayan and D. J. Mooney, Alginate Hydrogels as Synthetic Extracellular Matrix Materials, *Biomaterials*, 1999, **20**(1), 45–53.

76 P. Prang, R. Müller, A. Eljaouhari, K. Heckmann, W. Kunz, T. Weber, C. Faber, M. Vroemen, U. Bogdahn and N. Weidner, The Promotion of Oriented Axonal Regrowth in the Injured Spinal Cord by Alginate-Based Anisotropic Capillary Hydrogels, *Biomaterials*, 2006, **27**(19), 3560–3569.

77 J. A. Rowley and D. J. Mooney, Alginate Type and RGD Density Control Myoblast Phenotype, *J. Biomed. Mater. Res.*, 2002, **60**, 217–223, DOI: **10.1002/jbm.1287**.

78 F. Brandl, F. Sommer and A. Goepferich, Rational Design of Hydrogels for Tissue Engineering: Impact of Physical Factors on Cell Behavior, *Biomaterials*, 2007, **28**(2), 134–146, DOI: **10.1016/j.biomaterials.2006.09.017**.

79 J. Peng, L. Li, Y. Nie, T. Liu and K. Song, 3D Bio-Printing Fabrication and Properties of Graphene Dispersion-Based Hybrid Scaffolds, *J. Phys. Conf. Ser.*, 2020, **1622**(1), 012062, DOI: **10.1088/1742-6596/1622/1/012062**.

80 T. A. Partridge, Tissue Culture of Skeletal Muscle, *Basic Cell Culture Protocols*, 1997, pp. 131–144, DOI: **10.1385/0-89603-441-0:131**.

81 Q.-Z. Chen, S. E. Harding, N. N. Ali, A. R. Lyon and A. R. Boccaccini, Biomaterials in Cardiac Tissue Engineering: Ten Years of Research Survey, *Mater. Sci. Eng., R*, 2008, **59**(1–6), 1–37, DOI: **10.1016/j.mser.2007.08.001**.

82 K. Y. Lee and D. J. Mooney, Alginate: Properties and Biomedical Applications, *Prog. Polym. Sci.*, 2012, **37**(1), 106–126, DOI: **10.1016/j.progpolymsci.2011.06.003**.

83 A. Sergeeva, A. S. Vikulina and D. Volodkin, Porous Alginate Scaffolds Assembled Using Vaterite CaCO3 Crystals, *Micromachines*, 2019, **10**(6), 357.

